

# 3D printed acoustic igniter of oxygen-kerosene mixtures for aerospace applications

Roman Marchan\*, Andrii Oleshchenko\*\*, Samir Vekilov\*\*\*, Mihaylo Arsenuk\*\*\*\* and Olexander Bobrov\*\*\*\*\*

*\*Firefly Aerospace*

*Ukraine, Dnipro, roman.marchan@fireflyaerospace.com*

*\*\*Firefly Aerospace*

*Ukraine, Dnipro, andrii.oleshchenko@fireflyaerospace.com*

*\*\*\*Firefly Aerospace*

*Ukraine, Dnipro, samir.vekilov@fireflyaerospace.com*

*\*\*\*\*Firefly Aerospace*

*Ukraine, Dnipro, mihail.arsenuk@fireflyaerospace.com*

*\*\*\*\*\*Firefly Aerospace*

*Ukraine, Dnipro, alexsandr.bobrov@fireflyaerospace.com*

## Abstract

The acoustic igniters based on Hartmann-Sprenger tube are being developed by Firefly Aerospace Ukraine for several propulsion concepts operating on LOX and Kerosene. The present paper describes the experimental study of such igniters. The stable ignition was confirmed within inlet pressure range from 10 to 120 bar and mixture ratio range from 0.5 to 8. The maximum cumulative firing time of one igniter was over 100 seconds. Such results were obtained through the application of kerosene regenerative cooling and optimization of kerosene injection system. All igniters were 3D printed using a selective laser melting method.

## 1. Introduction

It was experimentally proven that acoustic igniters based on Hartmann-Sprenger tube can be used for ignition of most aerospace propellant combinations [1, 2, 3, 4, 5]. However, despite the numerous promising experimental results, so far, such igniters are mostly considered as prospective candidates for the replacement of existing ignition systems. This can be explained by several reasons. Firstly, acoustic igniters are vulnerable to overheating which reduces their firing time. It is especially the case with respect to rocket propellants and high operation pressures. The existing igniter designs make it difficult to apply sufficient cooling system. Secondly, acoustic igniters require availability of compressed gas to provide supersonic expansion inside igniter. Most of the known test results regarding the acoustic igniters were achieved under moderate operation pressures (up to 20 bar). High operation pressures, which are typical for rocket combustors, lead to increasing gas flow rate through igniter in comparison to moderate operation pressures. As a result, the gas storage system can be inappropriately large and heavy. Hence, miniaturization of acoustic igniters is a desirable option. The miniaturization also facilitates integration of igniters into combustor designs.

Additive manufacturing methods provide extra possibilities in development of acoustic igniters. First of all, it is a possibility to manufacture regenerative cooled structure with complex shape. Secondly, additive manufacturing allows rapid implementation of design changes, which is important for experimental optimization of the design.

Thus, the research presented in this paper was focused on the following issues:

- Regenerative cooling of igniter;
- Minimizing igniters size;
- High pressure operation;
- Using additive manufacturing.

## 2. Igniter designs

The basic scheme of Hartmann-Sprenger tube (HST) is depicted on Fig. 1. Geometrical parameters  $d$ ,  $D$ ,  $S$ ,  $L$  and resonance tube inner shape should correspond to some optimum combinations which provide maximum heat generation. Based on the previous research results [1] the following relations were chosen in the present study:  $S/d=2.0\dots2.4$ ,  $D/d=1.4\dots1.6$ ,  $L/d=8\dots9$ . The resonance tube inner shape was chosen as a combination of conical inlet section and cylindrical end section (Fig.2), which is also based on the experimental results described in research [1].

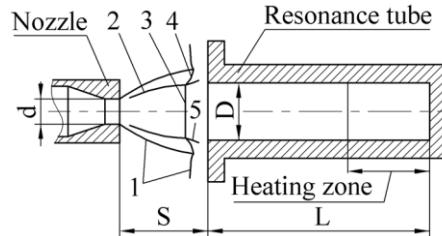


Figure 1: HST basic scheme: 1- gas jet boundary; 2- oblique shock; 3- Mach disc; 4- reflected shock; 5- boundary of internal subsonic zone.

Application of additive manufacturing methods requires certain adaptation of igniter design in order to provide, at least, its printability. In addition, there was a goal to get “ready for use” igniter structure just after printing with minimum post-printing procedures. Thus, keeping the abovementioned geometrical relations and manufacturing goal, the HST design was converted into the form presented on Figure 2.

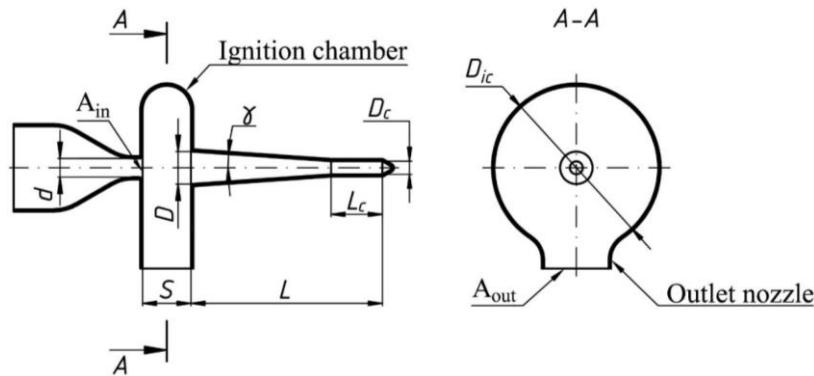


Figure 2: HST geometry used for igniters.

In comparison to HST on Fig.1 the HST on Fig.2 has two additional components which are an ignition chamber and outlet nozzle. The ignition chamber geometry should provide two functions: proper interaction of gas jet with resonance tube and stable combustion process. The size of outlet nozzle determines the jet expansion ratio which should correspond to the chosen HST geometrical parameters. Jet expansion ratio can be determined as a ratio between gas total pressure at inlet nozzle and static pressure in ignition chamber ( $P_{in}/P_{ic}$ ). Pressure ratio range  $P_{in}/P_{ic}=5.5\dots6.5$  was chosen which, according to research [1], corresponds the maximum experimentally measured temperature increase in a resonance tube. The pressure ratio  $P_{in}/P_{ic}$  is approximately equal to the area ratio between outlet and inlet nozzles ( $A_{out}/A_{in}$ ). Thus, the size of igniter outlet nozzle should be within the range  $A_{out}/A_{in}=5.5\dots6.5$ . Flow speed in the outlet nozzle becomes sonic (choked mode) if inlet pressure  $P_{in}$  exceeds certain value which depends on  $A_{out}/A_{in}$ . Jet expansion ratio inside HST is independent on inlet and ambient pressures on choked modes, which stabilizes heating process inside a resonance tube.

The igniter size mostly depends on inlet nozzle area  $A_{in}$ . It means that minimization of inlet nozzle diameter results in minimization of HST size. The following versions of HST were planned to be tested:  $d=3.8, 2.4, 1.8, 1.3$  and  $0.9$  mm. The shape of resonance tube cavity and its specific length  $L/D$  were also chosen based on the previous research [1]. The conical resonance tube inlet provides higher heating temperatures and makes heating less sensitive to the variation of  $S/D$  [6, 7].

Converting HST to igniter means, at least, adding a fuel injection system to the ignition chamber. Additionally, the regenerative cooling system should be implemented in order to provide igniter long-time operation. Providing of fuel injectors and cooling channels by means of additive manufacturing has some limitations. One of them is repeatability of hydraulic characteristics: channel friction losses, discharge coefficient of orifices and flow pattern of injectors.

Special experimental studies were performed by Firefly Aerospace regarding this issue. The several specimens of fluid ducts were 3-D printed of Inconel 718 using EOS M400 printer (Table 1). The flow passages and their inlet/outlet edges were not subjected to any post-printing mechanical treatments.

The specimens were subjected to water flow tests under the following pressure drops: 5, 10, 15 and 20 bara. It was observed that the flow pattern depends mainly on channel diameter and actual shape of outlet edge rather than pressure drop and channel specific length  $l/d_c$ . That is why pictures in Table 2 were chosen voluntarily independently on  $l/d_c$  and pressure drop. The pictures demonstrate unpredictable behaviour of water jets for the specimens with  $d_c=0.5, 0.6$  and  $0.8$  mm. The specimens with  $d_c=1.0$  mm produce much more repeatable cylindrical jets. Based on these results it was decided that fuel injection into ignition chamber should be performed via simple round holes with diameter not less than 1 mm.

Table 1: 3-D printed duct specimens for water hydraulic tests

$d_c$ , mm	$l/d_c$	Quantity
0.5	1	5
0.5	2	5
0.5	6	4
0.6	1	5
0.6	2	4
0.6	6	5
0.8	0.5	5
0.8	1	4
0.8	2	5
0.8	6	5
1	0.5	5
1	1	5
1	2	5
1	6	5

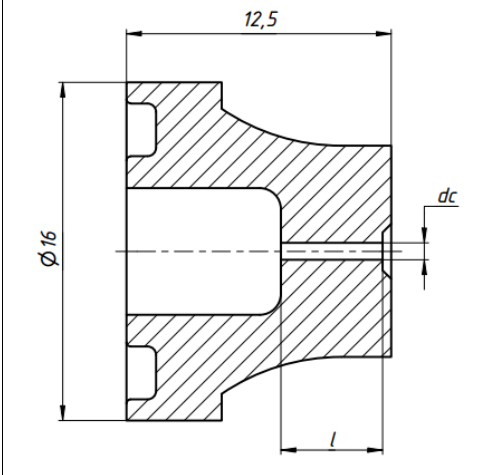










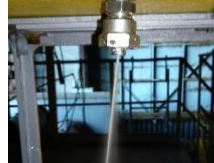











Table 2: Water flow patterns at the outlet of specimens

$d_c$ , mm	Specimen number				
	1	2	3	4	5
0.5					
0.6					
0.8					
1.0					

Repeatability of hydraulic resistance of the 3D printed specimens was assessed via flow coefficient:

$$C_v = m / \sqrt{2 \cdot \rho \cdot \Delta P} \quad (1)$$

Where:  $m$  – mass flow rate,  $\rho$  - density,  $\Delta P$  – pressure drop.

The water flow tests demonstrated much better repeatability of  $C_v$  for the channels with channel diameter  $d_c=1\text{mm}$ . As an example, Table 3 shows the measured variations of  $C_v$  from average values for  $l/d_c=6$  and  $\Delta P=10$  bar. Repeatability of 1 mm channels in “as printed” conditions seems to be on an acceptable level. However, this result was obtained on the simple straight channels and in case of complex geometry the additional analysis is necessary. Meanwhile it was decided that minimum size of the igniters’ cooling channels should not be less than 1 mm.

Table 3: Deviation of  $C_v$  for the channel specimens with  $l/d_c=6$  under  $\Delta P=10$  bar

$d_c$ , mm	0.5	0.6	0.8	1.0
$\Delta C_v$ , %	-30...+37.8	-25...+20.6	-17...+9.8	-2.2...+1.6

Different regenerative cooling schemes were considered. Among them two schemes depicted on Fig.3 were chosen for manufacturing and tests. Since that it is regenerative cooling the fuel injection was coupled with cooling passages. The fuel injection, in general, is similar to the previous researches [1, 2]. However, the specific feature of fuel injection according to Fig.3 is a presence of two injection ports. There is a time difference between fuel injections for these ports during igniter start-up which should minimize pressure peaks after ignition.

The basic CFD analysis of fuel flow was performed in order to optimize channels geometry in terms of proper velocities distributions and minimizing flow separation zones. The CFD calculations for two cooling schemes with optimized channels are shown on Fig.4.

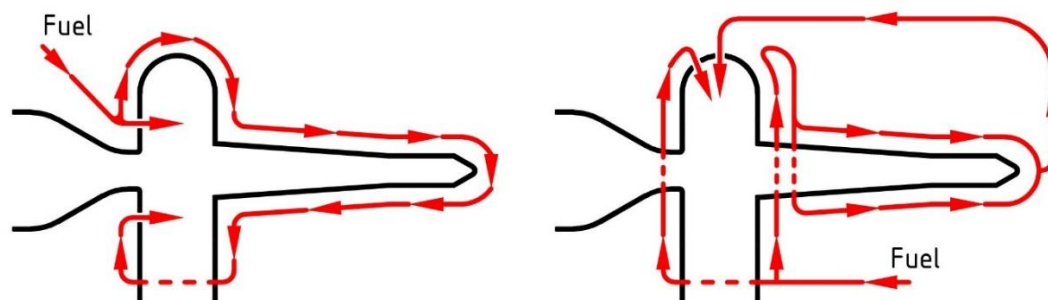


Figure 3: Regenerative cooling schemes

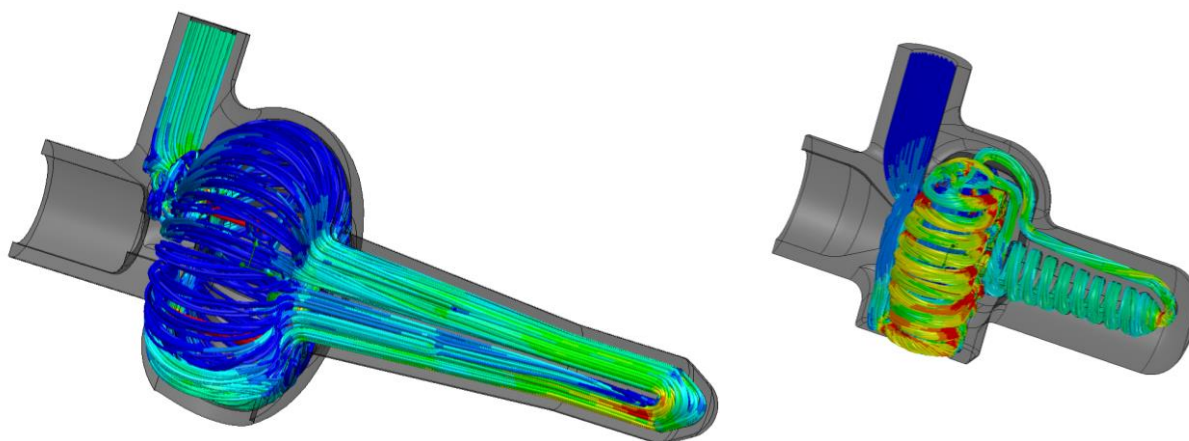


Figure 4: CFD visualization of fuel streamlines in cooling channels (the left picture shows an igniter with  $d=3.8$  mm, the right one is an igniter with  $d=1.8$  mm)

The cross-section views of igniter with  $d=1.8$  mm are shown on Fig. 5. Its cooling scheme corresponds to the right scheme from Fig. 3. Most of the igniters had the same cooling scheme except for igniters with  $d=3.8$  mm and  $d=2.4$  mm.

The inner wall thickness is a critical parameter for the cooling effectiveness. Acceptable wall thickness depends on thermal conductivity of construction material. It was planned to use high strength Inconel 718 and CoCr alloy which



have low thermal conductivity. Based on previous Firefly Aerospace experience with 3D printing of these alloys the thickness 0.4 mm was chosen.

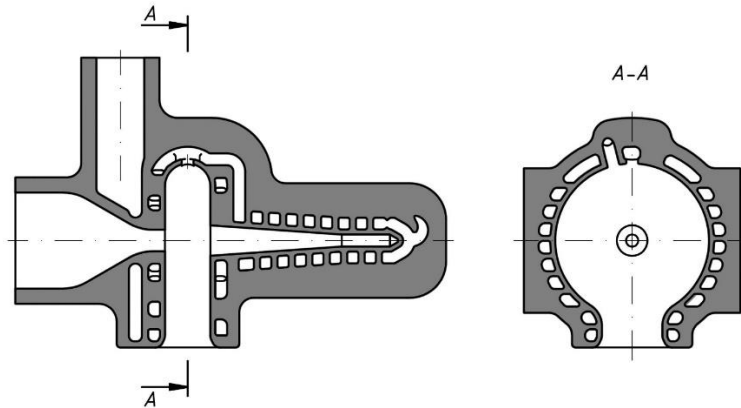


Figure 5: Cross-sectional views of an igniter with  $d=1.8$  mm.

Manufacturing of the igniters was performed on two 3D printers: EOS M400 and Sisma Mysint100. The igniters printed on EOS M400 were made from Inconel 718. The igniters printed on Sisma Mysint100 were made from CoCr alloy. The fuel channels were not subjected to any post-printing treatments (except powder removing). Regarding the oxygen inlet nozzle, it was determined that in case of Inconel 718 the mechanical calibration of nozzle is required. The shapes of oxygen nozzle of CoCr igniters were on acceptable level and were not calibrated. The machined connectors were TIG welded to igniters to provide mechanical interface with test facilities. Fig. 6 demonstrates the igniters on a building plate just after printing and Fig. 7 demonstrates the igniters ready for the tests.

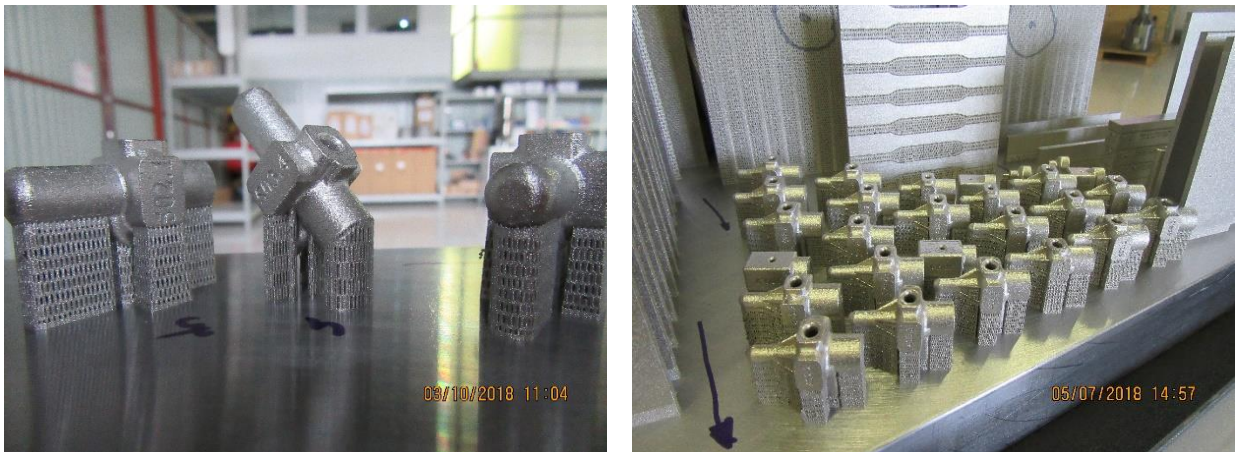


Fig. 6: Printed igniters on a building plate (Inconel 718, EOS M400).



Fig. 7: Manufactured igniters (from left to right):  $d=3.8$  mm,  $d=2.4$  mm,  $d=1.8$  mm,  $d=1.8$  mm CoCr,  $d=1.3$  mm,  $d=0.9$  mm.

### 3. Firing test facility

The firing test facility (Fig.8) consists of three feed systems: gaseous oxygen, kerosene and gaseous nitrogen. The nitrogen feed system provides pre-start and post-firing purging. Independent purging of both oxygen and kerosene lines can be performed. The kerosene 36 litres tank is pressurized by nitrogen. The maximum supply pressures at the igniter inlets are 130 bar for kerosene and 120 bar for oxygen. Such pressure level allows to test igniters at the conditions which are close to the rocket combustors. For example, pressure in combustion chambers and gas-generators of liquid rocket engines operated according to gas-generator cycle normally does not exceed 100 bar. The following measurement accuracies are provided: pressure  $\pm 1\%$ , kerosene flow rate  $\pm 1\%$  and temperature  $\pm 1^\circ\text{C}$ . Oxygen mass flow rate is determined via measured inlet pressure  $P_o$  and temperature  $T_o$  [8]:

$$m_o = 0.04 \cdot C_d \cdot \frac{P_o \cdot A_{in}}{\sqrt{T_o}} \quad (2)$$

Where:  $C_d$  – oxygen nozzle discharge coefficient,  $P_o$  and  $T_o$  – stagnation values of pressure and temperature at the nozzle exit.

The static values of  $P_o$  and  $T_o$  are measured. However, due to very low gas velocity at the points of measurements, it is possible to use the measured static values in equation (2) without any corrections.

Discharge coefficient  $C_d$  depends on nozzle geometry and its operation mode. The available experimental data were used to define  $C_d$  [8].

Equation (2) is applicable only for choked operation mode which is the case only before ignition. After ignition the flow through the oxygen nozzle becomes subsonic and equation (2) is not valid.

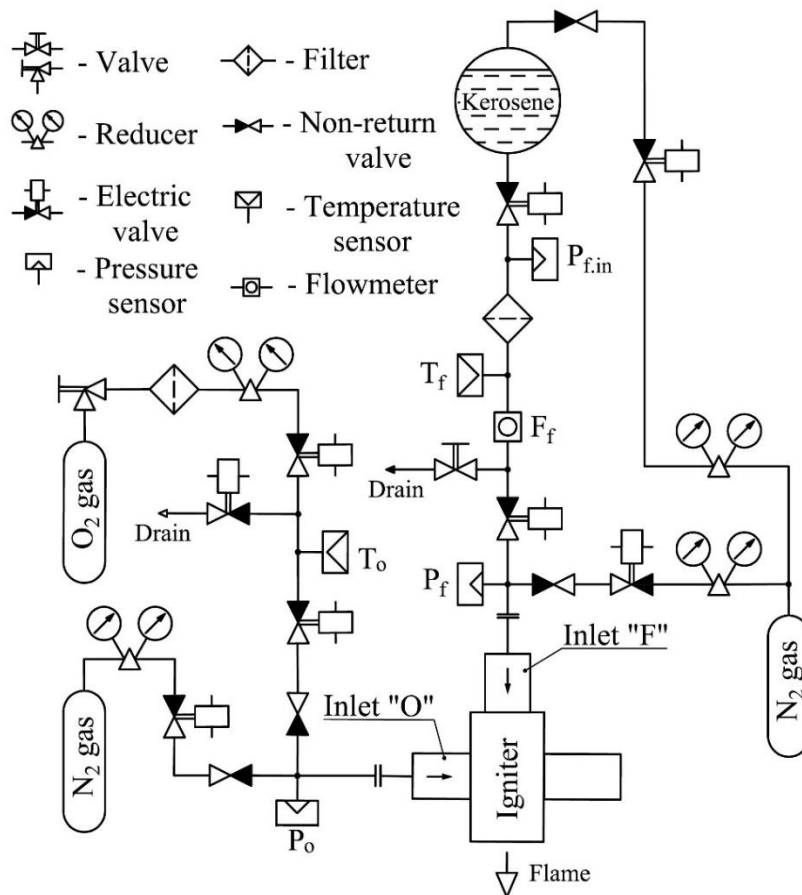


Figure 8: Firing test facility layout.

## 4. Test campaign

### 4.1 Water flow tests

All manufactured igniters were subjected to water flow tests in order to determine the flow coefficients  $C_v$  of cooling ducts (Eq. (1)). Actual values of  $C_v$  were used to adjust kerosene inlet pressure according to predetermined mixture ratio (MR). It should be noted that MR can be more or less precisely tuned only before ignition (start-up mode). After ignition MR can decrease or increase depending on inlet pressures, actual  $C_v$  and combustion efficiency.

The water flow tests showed that  $C_v$  differences between same igniters are bigger than for the 3D printed 1 mm channel specimens (Tables 1 and 3). Deviations of  $C_v$  for the most cooling ducts were in the range of  $\pm 5\%$ .

### 4.2 Firing test procedures

Different test procedures were implemented. Among them the most noticeable ones are described below.

Test procedure #1:

1. Switch-on the  $N_2$  purging of both oxygen and kerosene lines.
2. Switch-on the oxygen supply and stop oxygen line purging. Kerosene line is continuing to purge.
3. Switch-on the kerosene supply and stop the kerosene line purging.
4. Firing operation.
5. Switch-off the oxygen and kerosene supply and simultaneously switch-on purging of both oxygen and kerosene lines.

Test procedure #2:

1. Switch-on the oxygen supply.
2. Switch-on the kerosene supply.
3. Firing operation.
4. Switch-off the oxygen and kerosene supply and simultaneously switch-on purging of both oxygen and kerosene lines.

Test procedure #3:

1. Switch-on the kerosene supply.
2. Switch-on the oxygen supply.
3. Firing operation.
4. Switch-off the oxygen and kerosene supply and simultaneously switch-on purging of both oxygen and kerosene lines.

Most of the tests were conducted according to procedure #1. The duration of firing operation was varied from 1 to 32 seconds. During the oxygen line purging the preheating of resonance tube takes place. Heating of resonance tube continues with oxygen after switching-off the oxygen line purging. So purging facilitates resonance tube preheating and potentially allows to exclude the preheating with oxygen.

Meanwhile, excluding the purging is desirable option as it allows to simplify the ignition system and reduce its mass. Procedures #2 and #3 were developed to check ignition operation without preliminary purging. Post-purging was not excluded for safety reasons (but it can be excluded in flight operation). These procedures were used only for high pressure tests. It is known that with increasing gas stagnation pressure the rate of heating and temperature in resonance tube increases [1, 6]. Absence of start purging means absence of resonance tube preheating with purge gas. It was supposed that under high pressure (about 100 bar) the rate of heat release would be sufficiently high to obtain acceptable ignition delay time. Procedure #2 is risky because oxygen enters the kerosene duct. That is why the time gap between steps 1 and 2 in test procedure #2 should be minimized.

### 4.3 Scope of tests

It was not obvious from the beginning that minimizing igniter size would be successful. Thus, the testing was started with the biggest igniters which have oxygen nozzle throat  $d=3.8$ . After successful tests of these igniters the igniters with  $d=2.4, 1.8, 1.3$  and  $0.9$  mm were subsequently tested. A similar situation was with the duration of firing operation.

The first tests were conducted with 1 second firing time and then with progressive increasing up to 32 seconds. Some igniters were subjected to multiple ignition tests.

The first igniters were 3D printed with Inconel 718 without any heat treatments. Thermal destruction of some igniters led to experiments with material heat treatments which should facilitate high temperature operation. Another option was using CoCr alloy instead of Inconel 718.

## 5. Result discussion

Most of the igniters with oxygen nozzle throat  $d=3.8, 2.4, 1.8$  and  $1.3$  mm demonstrated the stable ignition withing the range of mixture ratio  $MR=1.5..4.0$  while the obtained ignition limits were  $MR_{min}=0.4$  and  $MR_{max}=8$ . When determening the ignition limits the unstable ignitions, ignitions with high delay time and explosions were taken into account. The igniters with  $d=0.9$  mm could not ignite the oxygen-kerosene mixtures so this size can be considered, at this moment, as a size limit. Most probably it is a result of technological (3D printing accuracy) limitation.

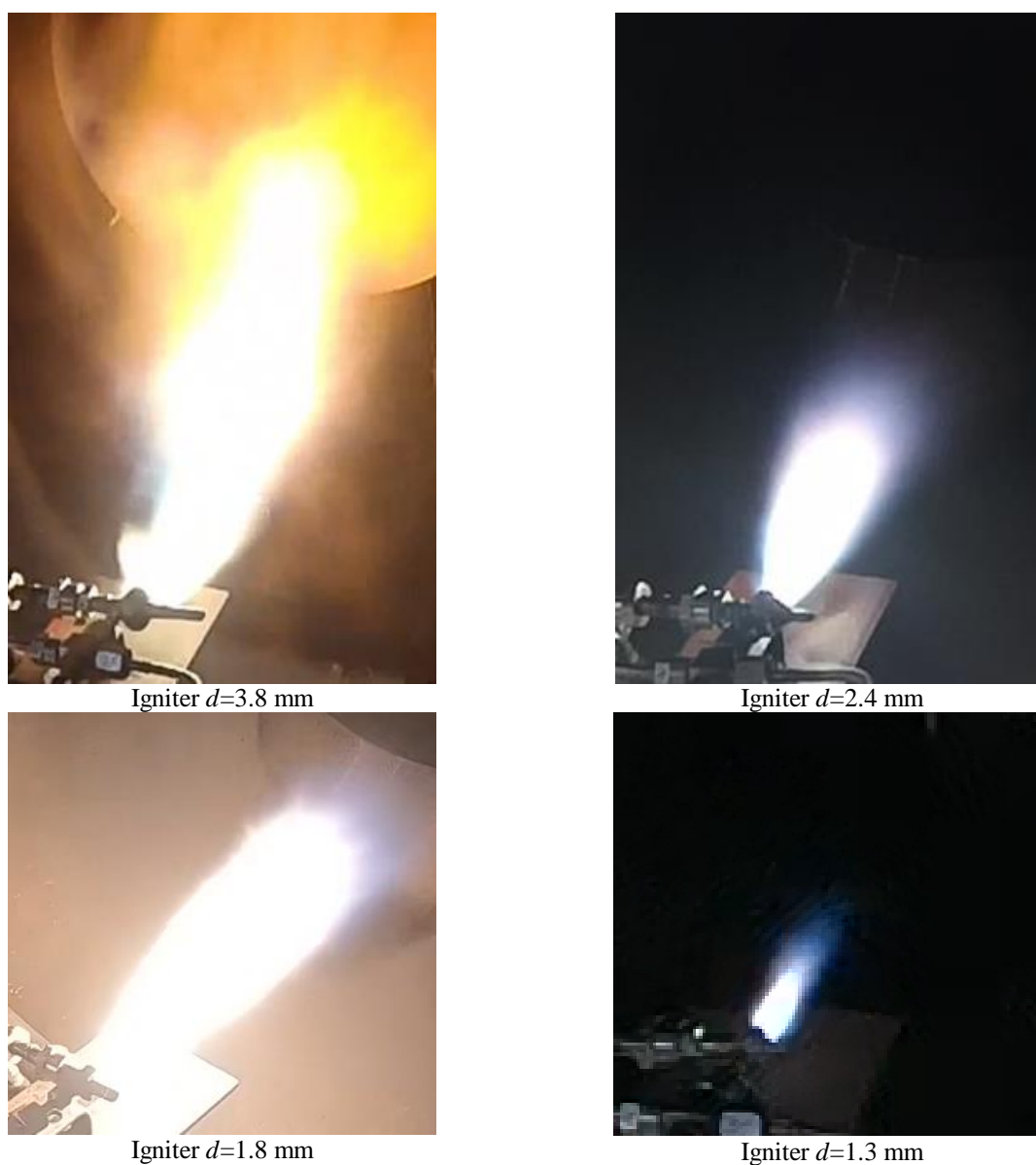


Figure 9: Igniters firing operation.

The following criteria of “normal” ignition were voluntarily established: stable ignition, stable combustion after ignition, absence of explosion and ignition delay time less than 0.2 seconds. Fig.10 demonstrates the inlet pressures



where the “normal” ignitions were obtained. Fig.10 collects tests with all igniters with  $d=1.3\text{...}3.8$  mm under  $MR=1.5\text{...}4.0$ .

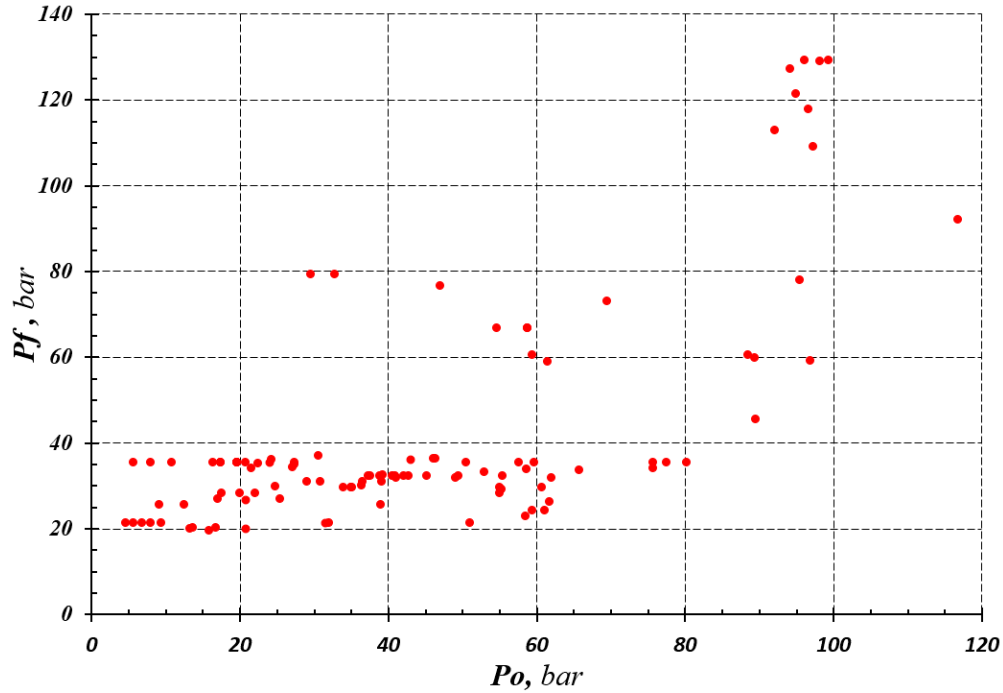


Figure 10: Ignitions vs oxygen inlet pressure  $P_o$  and fuel inlet pressure  $P_f$  under  $MR=1.5\text{...}4.0$ .

The ignition delay time was determined based on the oxygen inlet pressure measurements. The firing tests according to procedure #1 demonstrated ignition delay time  $\approx 0.04$  seconds which was repeatable over wide range of inlet pressures and mixture ratio. Fig.11 shows inlet pressure records during firing test of igniter with  $d=1.8$  mm. Firing time during this test was 5 seconds. Fig.12 demonstrates test of another igniter sample with firing time 32 seconds. The similar ignition delay time was recorded.

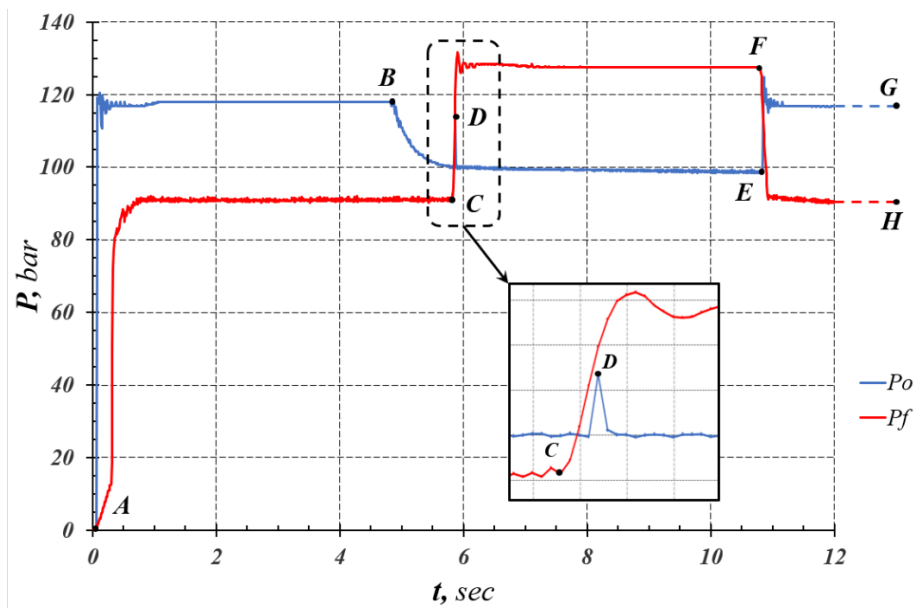


Figure 11: Inlet pressures measurement during firing test of igniter with  $d=1.8$  mm (AB, EG –  $N_2$  purging of  $O_2$  duct; AC, FH –  $N_2$  purging of kerosene duct; BE – Supply of  $O_2$ ; CF – Supply of kerosene; D – Ignition; CD – Ignition delay  $\approx 0.04$  sec; DE – 5 sec firing operation).

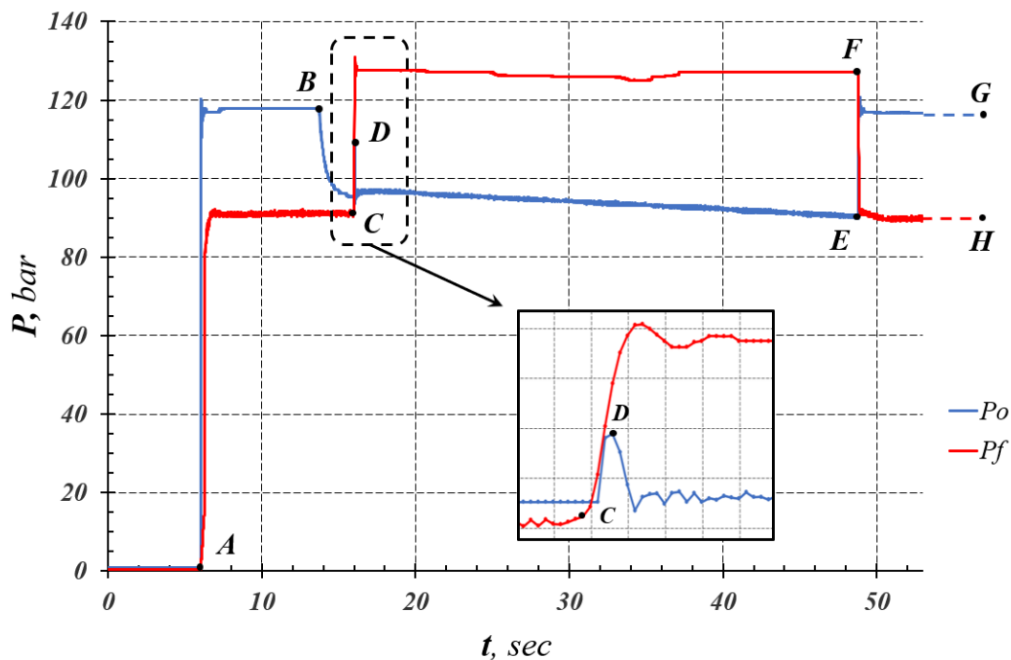


Figure 12: Inlet pressures measurement at high duration firing test of igniter with  $d=1.8\text{mm}$  (AB, EG –  $\text{N}_2$  purging of  $\text{O}_2$  duct; AC, FH –  $\text{N}_2$  purging of kerosene duct; BE – Supply of  $\text{O}_2$ ; CF – Supply of kerosene; D – Ignition; CD – Ignition delay  $\approx 0.04$  sec; DE – 32 sec firing operation).

As it was mentioned above, the firing tests according to test procedures #2 and #3 (without start-up purging) were conducted under high inlet pressures. Firing tests according to test procedure #2 were followed by igniter explosions. The explosions occurred just after supplying the kerosene to the igniter. Most probably the explosion happened in the cooling duct around the resonance tube. According to procedure #2 the oxygen enters the igniter before kerosene. Resonance tube is heated by oxygen and, at the same time, oxygen enters the kerosene cooling duct. When kerosene reaches the hot zone around the resonance tube it reacts with oxygen causing explosion. These results indicate the importance of kerosene line purging in test procedure #1.

According to test procedure #3 kerosene enters the igniter before oxygen. Thus, the presence of oxygen inside kerosene cooling duct was prevented. The ignition was obtained after supplying oxygen with ignition delay time  $\approx 0.14$  seconds (Fig.13). This time can be treated as time of reaching the ignition temperature in the resonance tube. As it can be noted, ignition delay time is significantly higher than for test procedure #1. This can be explained that the resonance tube in test procedure #1 is already preheated with purging gas and oxygen before supplying kerosene.

It should be noted that test procedure #3 provides so-called hard ignition. The pressure measurements presented in Fig.13 show about 30 bar pressure rise after ignition at the oxygen nozzle inlet. The tests according to procedure #1 were also followed by pressure peaks after ignition but the pressure rise was two times lower (Fig. 11, 12).

Effectiveness of regenerative cooling can be assessed via cumulative time of igniter firing operation. The cumulative firing time for one igniter with  $d=2.4$  mm exceeded 100 seconds and that igniter remained fully functional. Several igniters passed multiple ignitions. As a maximum number, 17 ignitions were obtained for one igniter with  $d=1.3$  mm. This igniter had 85 seconds cumulative firing time. The total firing operation time for all successfully tested igniter was 562 seconds. So, in general, the effectiveness of both cooling schemes, depicted on Fig.3 was proven.

After-test visual inspections of ignition chamber walls revealed that all igniters had the ablation of metal in the throat of exit nozzle (Fig.14, 15). In the most cases the ablation did not cause the leakage of kerosene. The ablation always took place within the first two seconds of firing operation. After this time the ablation stopped if it did not cause the kerosene leakage. The left picture on Fig.16 demonstrates the burning of metal particles produced by ablation at the beginning of firing operation. The subsequent normal operation of this igniter during the same test is shown on the right picture on Fig.16.

In some cases, the kerosene leakages occurred. The leakages caused the lack of coolant and, as a result, further thermal destructions of the igniters. Nevertheless, the igniters with leakage usually survived the first firing test. Fig.17 demonstrates the destruction of ignition chamber caused by leakage in the outlet nozzle.

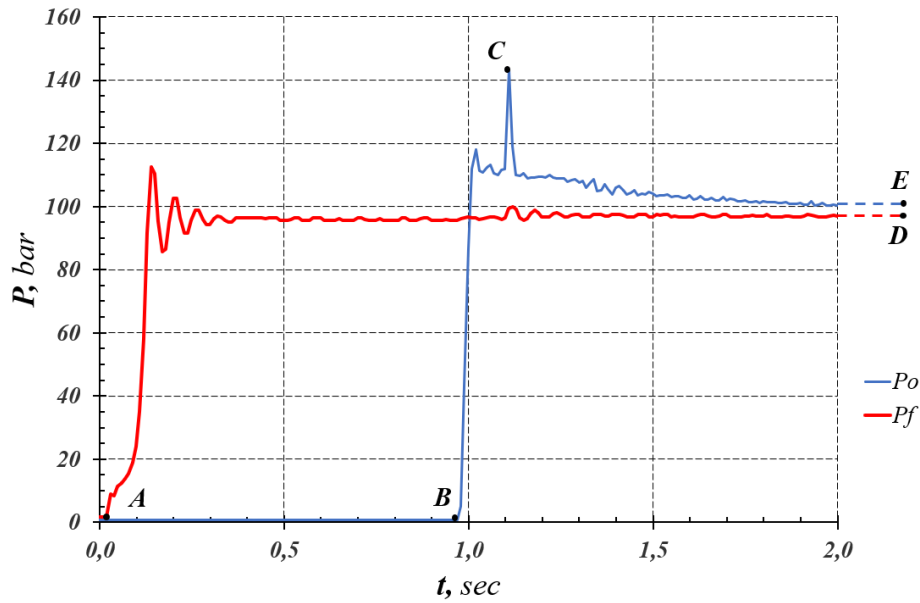


Figure 13: Inlet pressures during ignition according to test procedure #3. (Igniter  $d=1.8$  mm; AD – Kerosene supply; AB – Delay of  $O_2$  supplying; BE –  $O_2$  supply; C – ignition; BC – ignition delay  $\approx 0.14$  sec).

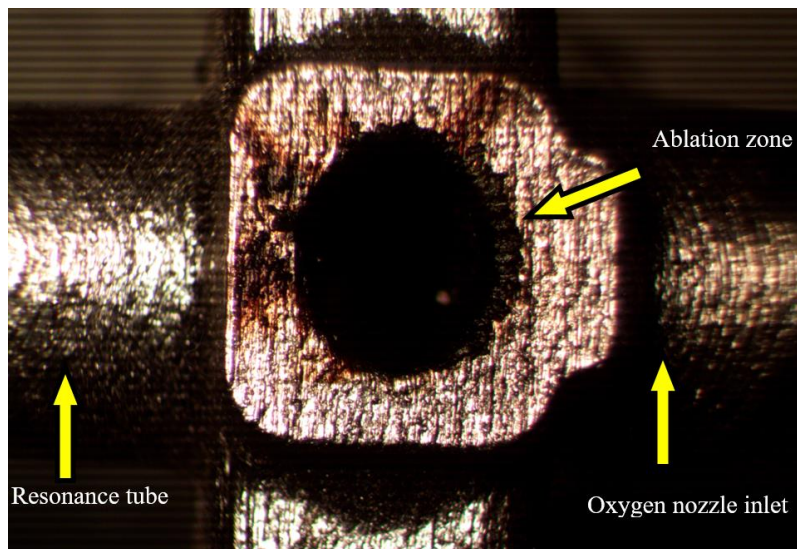


Figure 14: Material ablation at the outlet nozzle of igniter  $d=1.8$  mm after firing test

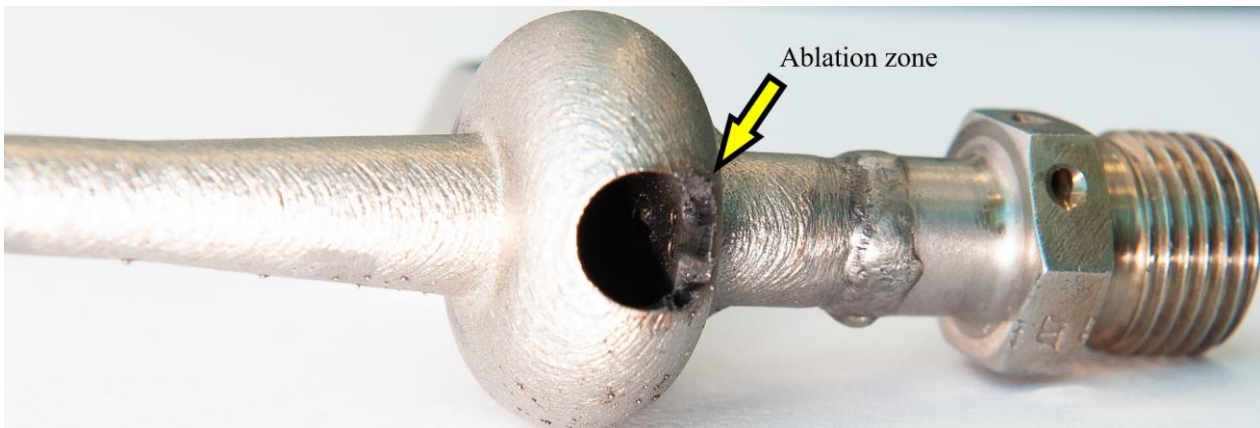


Figure 15: Material ablation at the outlet nozzle of igniter  $d=3.8$ mm after firing test



Figure 16: Ablation of metal just after ignition (left) and subsequent normal igniter operation (right)

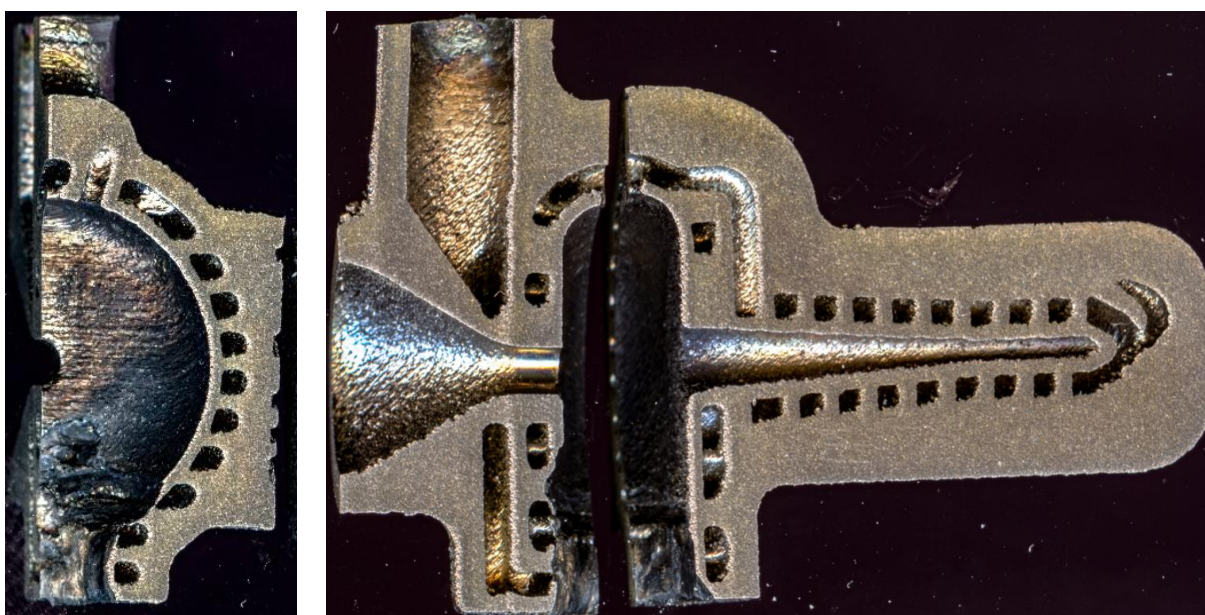


Figure 17: Thermal destruction of the ignition chamber wall caused by coolant leakage in the throat of the outlet nozzle

Special heat treatment of 3D printed Inconel 718 should improve its mechanical properties at high temperature operation [9]. However, firing tests of heat treated igniters did not show any advantages.

Igniters made from CoCr alloys demonstrated noticeably better resistance to the material ablation. The ablation was not excluded for CoCr but it was reduced.

It was observed that material ablations always took place in the same zone. It is a part of the outlet nozzle area placed on the oxygen inlet nozzle side. At the same time the opposite side of the outlet nozzle was in perfect condition (in cases when kerosene leakages were absent). In order to understand the cause of this problem, a picture of the damaged zone was compared with CFD oxygen flow visualization (Fig.18). The CFD picture shows that the ignition chamber and outlet nozzle from the side of resonance tube are covered with oxygen flow which creates a kind of film cooling. The opposite sides have zones without such film cooling effects. It is more clearly demonstrated by CFD visualization on Fig.19. Since that unsteady CFD simulation was performed, the Fig.19 shows the averaged surface streamlines. As it can be seen, the ablation zone exactly corresponds to area of peripheral vortexes interaction and this area does not have oxygen film cooling. Actually, the area without film cooling is much bigger but part of this area which is adjacent to the throat of outlet nozzle is subjected to the highest heat fluxes from combustion products. This fact is well known from the analysis of heat fluxes in rocket thrust chambers [9].

It should be also noted that combustion efficiency inside the ignition chamber was not estimated but it definitely must be low. The reason for this is low residence time of combustion products inside the ignition chamber in comparison to, for example, rocket combustors. The more convenient parameter which can be used instead of residence time is



combustor characteristic length  $L^*$  [9]. For the tested igniters this parameter can be written as  $L^* = V_{ic}/A_{out}$  where  $V_{ic}$  is volume of ignition chamber. Typically,  $L^*$  is expressed in meters. That is why  $V_{ic}$  should be expressed in  $m^3$  and respectively outlet nozzle area  $A_{out}$  should be in  $m^2$ . All the tested igniters have  $L^* = 0.04 \dots 0.07$  m which is, at least, 10 times lower than for rocket combustors [9]. Low combustion efficiency is acceptable for the igniter but, at the same time, it facilitates the cooling due to decreasing heat release inside igniter.

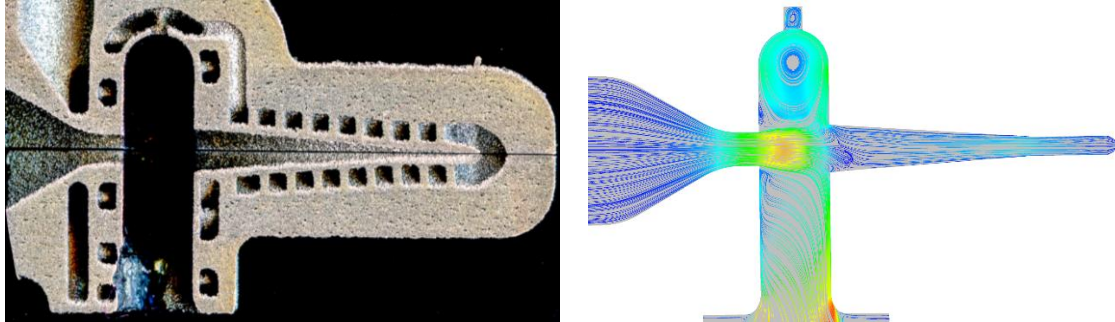


Figure 18: Damaged igniter with  $d=1.8$ mm (left) and streamlines according to CFD simulation of oxygen flow (right)

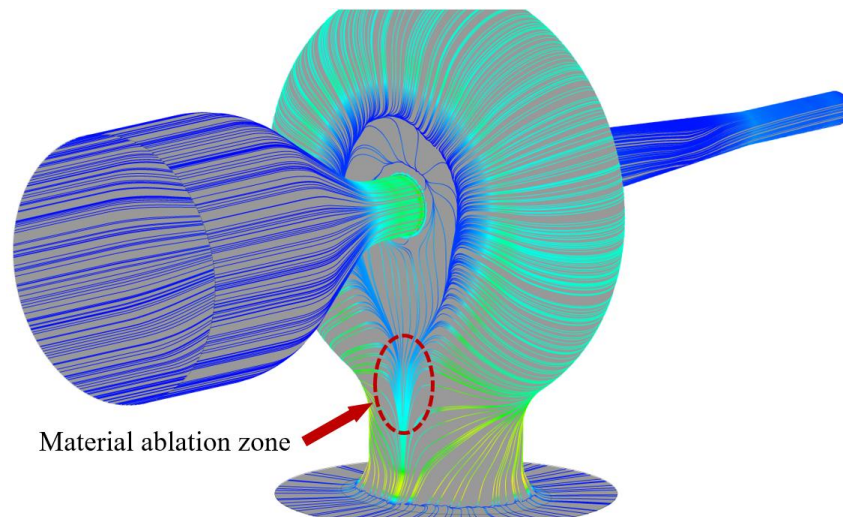


Figure 19: CFD picture of averaged surface streamlines and zone of material ablation during firing tests

Cooling effectiveness also depends on igniter operation modes and, in particular, on mixture ratio. Most of the igniters were tested at  $MR=1.5 \dots 2.5$ . This range can be recommended from the cooling point of view. Tests with  $MR > 3.0$  sometimes caused additional thermal destruction of igniters which were successfully tested at lower MR.

## 6. Conclusions

- Acoustic igniters with significantly different size were successfully manufactured using SLM additive manufacturing method. The adaptation of igniter design to the SLM process was performed.
- Additive manufacturing allowed the implementation of kerosene regenerative cooling of igniter structures.
- Igniters firing tests demonstrated the reliable ignition in wide range of mixture ratio and inlet pressures. The feasibility of kerosene regenerative cooling was confirmed.
- Regenerative cooling provides longtime igniters operation with multiple ignitions.
- Successful igniters high pressure operation indicates the applicability of acoustic igniters for the liquid rocket engines with turbopump feed system.
- Ignition without preliminary purging of igniter ducts was confirmed.
- The problem of high temperature material ablation was revealed in the course of firing tests. This problem was analyzed using CFD simulation. The correlation between ablation zone and oxygen flow pattern was found. This fact can explain the presence of ablation zone.



- Further research efforts should be focused on solving material ablation problem. The two options can be considered: optimization of ignition chamber inner shape and using alternative construction materials.

## References

- [1] Marchan, R. 2011. Small-scale supersonic combustion chamber with gas-dynamic ignition system. *Combustion Science and Technology*. 183(11): 1236-1265.
- [2] Niwa, M., Kessaev, Kh., and Santana, A. 2001. Development of a Resonance Igniter for GO/Kerosene Ignition. *Journal of Propulsion and Power*. 17(5): 995-997.
- [3] Marchese, V. 1974. Development and demonstration of flueric sounding rocket motor ignition. Report NASA CR-2418. Langley Research Centre.
- [4] Bogdanov, V. 2015. Contemporary achievements in the field of acoustic ignition systems. *Procedia Engineering*. 129: 702-707.
- [5] Lungu, P., Baurer, C., and Haidn, O. 2018. Operational behaviour investigation of Hartmann-Sprenger Tube based resonance ignition systems for oxygen/methane in-orbit propulsion applications. In conference: *Space Propulsion 2018*. SP2018-00229.
- [6] Kuptsov, V., Ostroukhova, S., and Filippov, K. 1977. Pressure fluctuations and heating of a gas by the inflow of a supersonic jet into a cylindrical cavity. *Fluid Dynamic* 5(12): 728-733.
- [7] Kuptsov, V., and Filippov, K. 1981. Pulsations of the pressure and heating of the gas when a supersonic jet enters a conical cavity. *Fluid Dynamic* 3(16): 468-470.
- [8] Lavrukhin, G.N. 2003. Nozzle aerogasdynamic. Vol.1 Nozzle internal characteristics. Moscow, Fizmatlit (in Russian).
- [9] Huzel, D.K., and Huang, D.H. 1992. Modern Engineering for Design of Liquid-Propellant Rocket Engines. AIAA.